Solitary wave-based delamination detection in composite plates using a combined granular crystal sensor and actuator

2015 Smart Mater. Struct. 24 125004

(http://iopscience.iop.org/0964-1726/24/12/125004)

IOP Publishing Smart Materials and Structures
Smart Mater. Struct. 24 (2015) 125004 (9pp) doi:10.1088/0964-1726/24/12/125004

Solitary wave-based delamination detection in composite plates using a combined granular crystal sensor and actuator

Eunho Kim[1], Francesco Restuccia[2], Jinkyu Yang[1,4] and Chiara Daraio[3]

[1] Aeronautics and Astronautics, University of Washington, Seattle, WA 98195-2400, USA
[2] Mechanical Engineering, Imperial College London, London SW7 2AZ, UK
[3] Mechanical and Processing Engineering, Swiss Federal Institute of Technology Zurich, Zurich 8092, Switzerland

E-mail: eunhokim80@gmail.com, f.restuccia14@imperial.ac.uk, jkyang@aa.washington.edu and daraio@ethz.ch

Received 12 May 2015, revised 15 September 2015
Accepted for publication 21 September 2015
Published 15 October 2015

Abstract

We experimentally and numerically investigate a diagnostic method for detecting hidden delamination in composite panels, using highly nonlinear solitary waves. Solitary waves are a type of nonlinear waves with strong energy intensity and non-distortive nature, which can be controllably generated in one-dimensional granular crystals. In this study, we use granular crystals as a combined sensor and actuator to detect hidden delamination in carbon fiber reinforced polymer (CFRP) composite panels. Specifically, we locally excite a CFRP composite specimen using the granular crystal as an actuator and measure the reflected waves that carry the specimen's diagnostic information using the same device as a sensor. We first investigate the effect of the panel's boundary conditions on the response of the reflected solitary waves. We then investigate the interactions of a solitary wave with delamination hidden in the CFRP composite specimen. Lastly, we define a damage index based on the solitary waves' responses to identify the location of the hidden delamination in the CFRP composite panel. The solitary wave-based diagnostic method can provide unique merits, such as portable and fast sensing of composites' hidden damage, thereby with the potential of being used for hot spot monitoring of composite-based structures.

Keywords: solitary wave, granular crystal, delamination

(Some figures may appear in colour only in the online journal)

1. Introduction

Fiber reinforced polymer (FRP) composites are widely used in numerous engineering applications, such as aerospace, civil, and renewable energy fields, owing to their high specific strength, stiffness, and corrosion resistance [1, 2]. However, their complex microstructure, composed of multiple layers of fiber and matrix, entail complex damage modes, e.g., fiber breakage, matrix crack, and delamination. One of the biggest challenges of the FRP composites stem from the fact that these damages are often invisible and difficult to diagnose.

In response to this, structural health monitoring (SHM) and nondestructive evaluation (NDE) of composite structures have been topics of active research for the past decades. A number of techniques have been proposed to identify hidden damages in composites. As for the SHM techniques, embedded or surface-mounted sensors have been widely investigated. For example, previous studies have shown that built-in piezoelectric ceramics can generate and record guided waves that interact with the damages in composites [3–6]. It has been also demonstrated that integrated fiber optic sensors

[4] Author to whom any correspondence should be addressed.

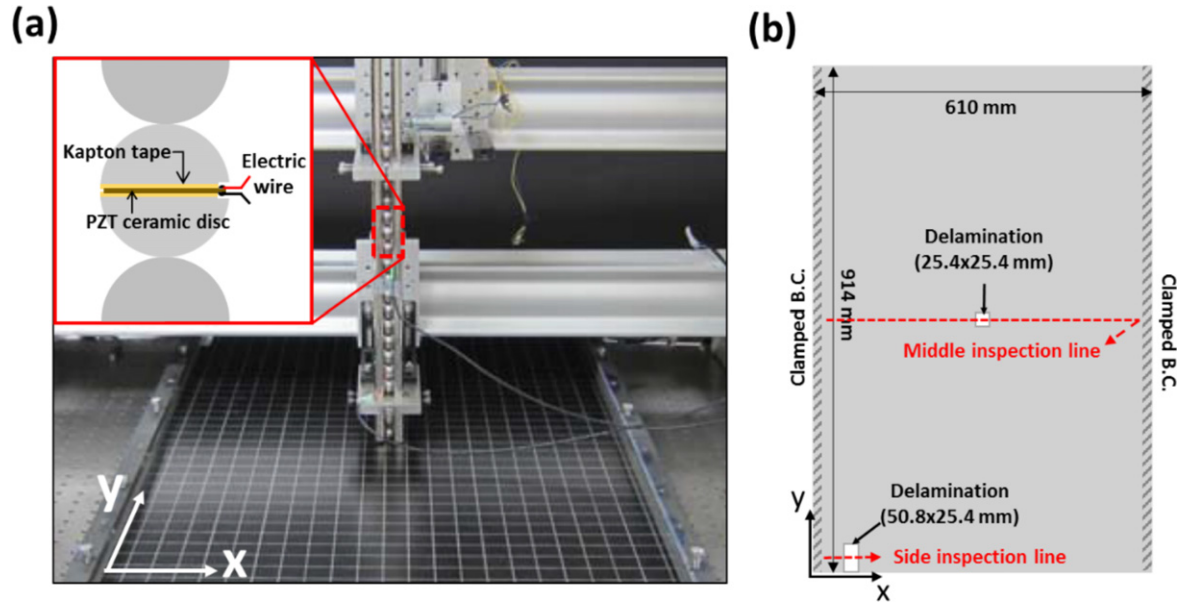

Figure 1. Experimental setup. (a) A granular crystal sensor/actuator prototype positioned at the center of the CFRP panel. Inset shows schematic of a sensor bead positioned in the seventh particle from the top of the chain. (b) Schematic of the CFRP panel with the location of fixture (shaded long edges), artificial delaminations (white boxes), and inspection lines (dashed red lines).

can monitor strain-field changes caused by damages in composite structures [7–9]. In regard to the NDE approaches, many techniques, including thermography, shearography, X-radiography, eddy current, ultrasonic C-scan, and scanning laser Doppler vibrometry have shown promising results [10–13]. However, each of these technologies has its own limitations that prevent wide usage of them in composites applications. In particular, the built-in sensors used for SHM add more complexity to host structures, often interfering with the functionality of the host structures and triggering false alarms. On the other hand, stand-alone inspection apparatuses for NDE are often bulky and expensive, limiting their accessibility to complex or hidden structural regions. There exist relatively simple inspection methods such as impact-echo and pulse-echo methods, but in complicated structures, it is hard to guarantee reliable diagnostic data due to their limited accuracy.

In this study, we investigate a diagnostic method based on a granular crystal sensor/actuator for fast and reliable inspection of delamination in composites. The granular crystal sensor/actuator is made of a one-dimensional chain of beads [14–16]. This chain supports the formation and propagation of highly nonlinear solitary waves, which are a type of nonlinear wave packets with compact waveforms [17, 18]. These solitary waves exhibit unique mechanical properties, such as high energy intensity, robustness, and controllable wave speed [19]. In this research, we excite carbon FRP composite samples with solitary waves via direct mechanical contact between the granular crystal and the FRP sample. The injected solitary wave excites the composite specimen locally, thereby creating stress waves that interact with the hidden delaminations in the panel.

The granular crystal performs not only as an actuator, but also as a sensor by measuring the reflected solitary waves generated from the interface between the granular crystal and the plate. Previous researches have reported that solitary waves' reflections are extremely sensitive to the material properties, geometry, and boundary conditions of the bounding medium [20–22]. Therefore, when used in composite diagnostics, we can assess the presence of delamination by interpreting the reflected solitary waves. In this research, we fabricate a carbon fiber reinforced polymer (CFRP) plate with hidden artificial delamination and conduct inspection mapping of this panel using a prototype of granular crystal sensor/actuator. We analyze the temporal profiles of reflected solitary waves and predict the locations of delamination based on the diagnostic signals contained in the reflected solitary waves. Also, we calculate a damage index to quantify the scattering of the reflected solitary waves. To understand the scattering behavior of the solitary waves, we numerically simulate their interaction with the delamination using finite element (FE) analysis. The experimental and numerical results indicate that the solitary wave-based diagnostic method is efficient in identifying hidden delamination underneath the inspection spots, making it suitable for quick hot spot monitoring of composite structures.

The rest of the paper is structured as follows: first, we describe the experimental setup in section 2 and numerical model in section 3. We show the interaction of a solitary wave with the pristine panel at various locations and discuss the effect of boundary conditions on wave reflection in section 4.1. The inspection results from the delaminations located at the center and the edge of the CFRP panel are discussed in sections 4.2 and 4.3, respectively. Lastly, in section 5, we conclude the paper with summary and future work.

2. Experimental setup

Figure 1 shows an experimental setup consisting of a granular crystal sensor/actuator prototype and a CFRP plate clamped at fixture. The granular crystal sensor/actuator is composed of 20 stainless steel beads (type-440C, elastic modulus $E = 200$ GPa, Poisson's ratio $= 0.26$, density $= 7800\,\mathrm{kg\,m^{-3}}$ [23]), which have an identical radius $R = 9.53$ mm and a mass $m = 28.2$ g. This chain of particles is supported vertically by four steel rods. We generate a solitary wave by applying mechanical impact on the top of the chain. For a consistent and controllable excitation, we drop a sphere (identical to the constituent beads of the chain) from a 5 mm height using a solenoid. The solitary wave propagating through the chain is measured by a sensor bead, which contains a calibrated piezoelectric ceramic disc (inset in figure 1(a)). Details of the sensor configuration and its calibration procedure can be found in [24]. The sensor bead is positioned in the seventh particle position from the top of the chain to allow enough distance from both the striker and the plate. The signal generated from the piezoelectric disc is recorded by an oscilloscope.

In this study, we test two CFRP panels: one with hidden artificial delamination and the other with no delamination, as a reference case. Both panels are manufactured using commercial grade carbon fiber prepregs (ACP Composite Inc.) with the layup angle of $[5(0/90)]_S$ and the dimensions of 914 mm × 610 mm × 4 mm as shown in figure 1(b). For the damaged plate, we include two artificial delamination defects at the center and in the corner of the plate (see figure 1(b)). These delaminations are created by embedding a single layer of 0.292 mm thin polytetrafluoroethylene (PTFE or Teflon) film in the middle of the laminate during the fabrication process. The central delamination is located at the exact center of the plate with a size of 25.4 × 25.4 mm, while the one in the corner is positioned 102 mm away from the side with a 50.8 mm × 25.4 mm size. The Teflon film in the corner is removed after the curing process, creating an empty slit between plies.

We fix long-edge sides of the CFRP panel using fasteners and clamps and scan the panel using the sensor/actuator unit attached in the movable supporting frame (figure 1(a)). To investigate the effect of panel's boundary conditions and the delamination, we scan the panel along the two inspection paths as shown by the dashed lines in figure 1(b). For the middle inspection path, we scan 19 points with 25.4 mm spacing, while in the corner path, we inspect 13 points with 10 mm spacing. For each inspection point, we conduct five measurements for statistical treatments, ensuring the repeatability of the acquired data.

3. Numerical model

We simulate the solitary wave propagation in the granular sensor/actuator and its interaction with the CFRP panel using a commercial FE program (ABAQUS/standard). Figure 2 shows a combined FE model of the granular sensor/actuator unit and the composite panel. For the composite panel, we use solid elements (linear brick element C3D8R) to account for the anisotropic mechanical properties of the CFRP material and the wave propagation in it. The elastic properties of unidirectional CFRP ply are $E_{11} = 143.4$ GPa, $E_{22} = E_{33} = 9.27$ GPa, $G_{12} = G_{13} = 3.8$ GPa, $G_{23} = 3.2$ GPa, $\nu_{12} = \nu_{13} = 0.31$, $\nu_{23} = 0.52$ where the subscript 1,2, and 3 represent the carbon fiber-, transverse of the fiber- and the thickness-directions of the ply, respectively [25]. The density of the composite panel is $\rho_p = 1850\,\mathrm{kg\,m^{-3}}$ according to the information provided by the ACP Composite Inc.

In granular crystals, the nonlinear Hertzian contact between particles is critical to generate solitary waves [16]. However, direct modeling of the spherical Hertzian contact using solid or axisymmetric planar elements requires an extremely fine mesh at the contact interface [26] (e.g., see the right inset of figure 2). FE simulations demand an extensive amount of computational resources and time. For the sake of efficiency, we simplify this spherical chain into point masses connected with nonlinear axial springs [17], as shown in the middle inset of figure 2. In this discrete element model, the nonlinear springs represent the Hertzian contact interaction between neighboring spheres (see the left inset of figure 2), whose force-displacement relationship can be expressed as $F = \beta\delta^{3/2}$ where F and δ are the contact force and an approach between the two particles, respectively. The contact coefficient β is defined as follows:

$$\beta = \frac{E\sqrt{2R}}{3\left(1-\nu^2\right)}, \tag{1}$$

where E, R, and ν are Young's modulus, radius, and Poisson's ratio of the sphere, respectively [27].

For the coupling between the last particle in the chain and the CFRP plate, we use solid elements (tetrahedral element C3D10) as shown in the right inset in figure 2. The choice of tetrahedral elements allows capturing the dynamic interaction between the last particle and the plate, because depending on the inspection point, the plate can develop not only out-of-plane (i.e., z-direction), but also in-plane motions. For the direct contact interactions at the interface, we use a penalty contact algorithm supported in ABAQUS/standard. To link this discrete element model with the full-scale FE model at the interface, we feed the nodal displacement information of the last particle into the central mesh of the last particle (see the inset of figure 2). Note that for the accuracy of the numerical simulations, we use a fine mesh near the contact region. This is to account for the local deformation and the corresponding stress concentration of the sphere in the vicinity of the contact region. For the computational efficiency, we use a minimal mesh density in this contact region, which is determined by a mesh convergence test. Here, we gradually increase the mesh density of the sphere and plate in the contact region and compare the contact behavior of the FE model with that from the Hertzian contact relationship [27]. We find the minimal mesh density that ensures the agreement with the analytical prediction.

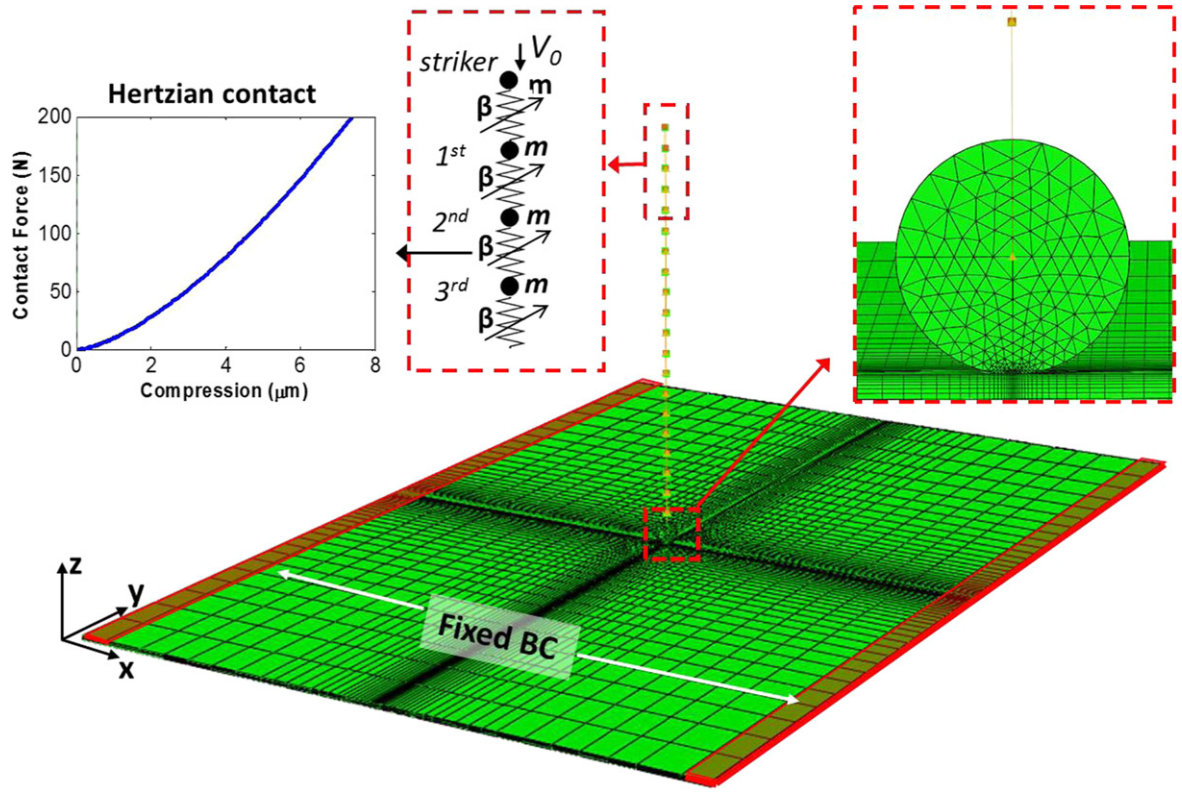

Figure 2. Finite element model of the granular crystal and the CFRP plate under contact. The insets show the Hertzian interaction relationship (left), the discrete element model of the granular chain (middle), and the contact model between the last particle in the chain and the CFRP plate (right).

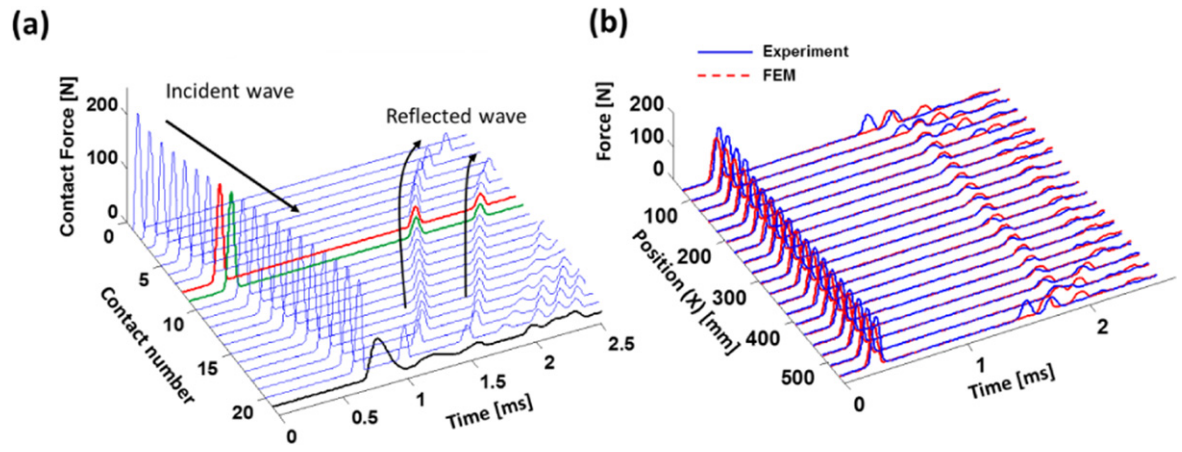

Figure 3. (a) Wave propagation in the granular crystal chain and its interaction with the pristine composite panel (b) Experimental force profiles in solid curves are measured from sensor bead located at the seventh bead position along the middle inspection path. The corresponding FE analysis results are also shown in dashed red curves.

4. Results and discussion

4.1. Boundary condition effect

Before we inspect the delaminated plate, we begin by investigating the responses of a solitary wave interacting with the pristine plate at various inspection points. Figure 3(a) shows the spatio-temporal plot of solitary waves propagating along the granular sensor/actuator, when it is positioned in the center of the pristine panel. Each curve represents the force profile calculated at every contact point between particles in the granular chain. For example, the first curve (from the left) shows the contact force between the striker and the topmost sphere in the chain. The last curve (black solid line in figure 3(a)) shows the force interaction between the last sphere and the composite panel. From this spatio-temporal map, we observe that a single solitary wave is generated upon the impact on the top of the chain and propagates down the granular crystal with a single-humped waveform (see the arrow indicating the incident wave in figure 3(a)). The solitary

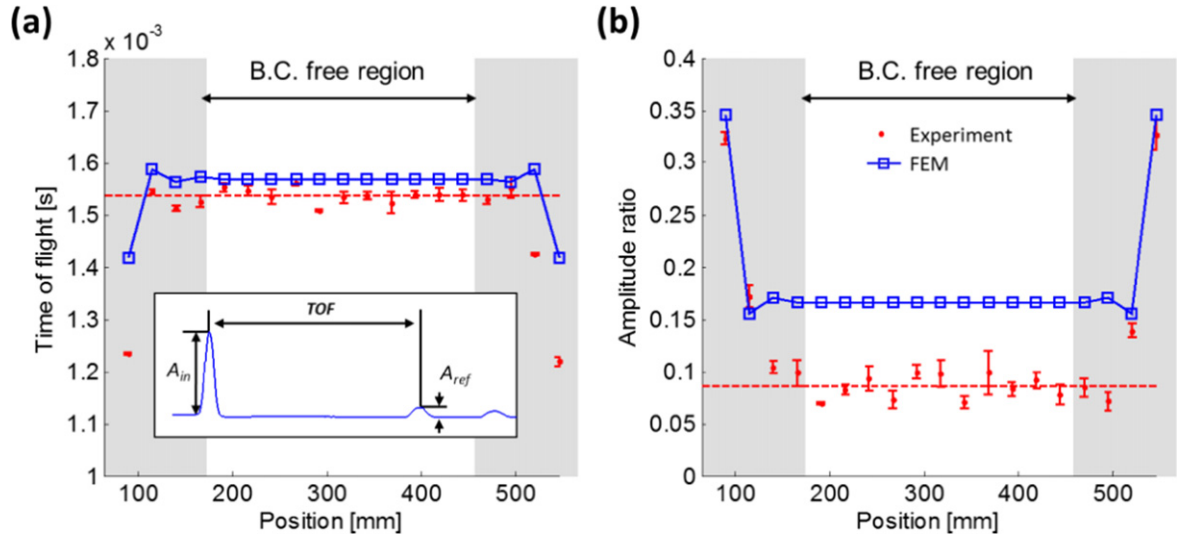

Figure 4. (a) Time of flight (TOF) of the first reflected waves measured at the seventh particle position. Inset shows how we quantify the TOF and the amplitude ratio. (b) Amplitude ratio of the first reflected wave with respect to the incident wave. Blue squares denote the FEM results, while the red dots with error bars show the average and the standard deviations of the experimental results.

wave propagating through the chain interacts with the composite panel at the bottom, and this interaction generates the formation of multiple wave reflections (see the arrows corresponding to these reflected waves).

Figure 3(b) shows the profiles of incident and reflected waves measured by the seventh particle (the location of the sensor bead in experiments), when inspecting the pristine panel along the central line of the plate. The first curve corresponds to the measurement from the smallest x-coordinate (see figure 1(b)), and the solid (dashed) curves represent experimental (numerical) results, respectively. It should be noted that the force profile recorded by the PZT-embedded sensor represents the average of the contact force felt at the two contact interfaces of the sphere [24]. Therefore, the numerical force history in figure 3(b) is identical to the average of seventh and eighth contact force profiles (red and green curves) in figure 3(a).

In figure 3(b), the first impulse, visible around 0.3 ms, is an incident solitary wave, while the subsequent impulses are reflected waves. For all the inspections conducted in this study, the waveform of the incident wave is identical due to the uniform excitation conditions of the granular crystal. However, the shape of the reflected waves varies depending on the location of the inspection point (e.g., distance from the clamped boundaries) or the presence of delamination underneath the inspection point. To analyze the boundary effects first, we calculate the time of flight (TOF) of the first reflected solitary wave, which is defined as the temporal distance between the incident and the first reflected waves, as shown in the inset of figure 4(a). We also calculate the amplitude ratio, which is the relative magnitude of the first reflected solitary wave to the incident one ($A_{\text{ref}}/A_{\text{in}}$). Figures 4(a) and (b) show the TOF and amplitude ratio as a function of the inspection position, respectively. It is obvious that the reflected solitary waves are significantly affected by the boundary condition of the composite panel. In the vicinity of the boundary, reflected waves exhibit shorter TOF and higher amplitude ratios. The authors' previous study on simple metallic plates has shown that such faster and stronger repulsion of solitary wave is attributed to the large coefficient of restitution expected when a spherical striker hits a plate near the fixed support [28]. In figure 4, however, if the inspection point is approximately 170 mm apart from the fixed boundary, the boundary effect becomes negligible and the responses of the first reflected solitary waves become identical regardless of the distance to the fixed boundary.

The boundary effect on the solitary waves' reflection can be explained by the behavior of the flexural waves propagating in the plate during the interaction time between the granular crystal and the plate. To calculate the interaction time of the last sphere with the panel, we consider a single spherical striker impacting on a flat plate. In this case, we can analytically obtain the contact time T_c [21, 28, 29]:

$$T_c = m^{2/5} V_0^{-1/5} A_p^{-2/5} \tau_c, \tag{2}$$

where m and V_0 are striker mass and velocity. A_p is a contact coefficient between the sphere and plate [27]:

$$A_p = \frac{4\sqrt{R}}{3}\left(\frac{1-v_s^2}{E_s} + \frac{1-v_p^2}{E_p}\right)^{-1}. \tag{3}$$

Here the subscripts s and p represent sphere and plate, respectively. τ_c is a dimensionless contact time obtained by solving a non-dimensionalized equation of motion for the sphere impacting on a plate (see [21, 28, 29] for details). We apply this analytical expression to the interaction of the granular chain with the composite panel by using an equivalent quasi-particle approach [30–32]. In the quasi-particle approach, we describe the solitary wave propagation —with a wavelength of approximately five particle diameters [17]—as the motion of a single particle having equivalent mass $m_e = 1.4m$ and velocity $V_e = 0.682V_0$, where m and V_0 are the single particle mass and striker's velocity [30–32].

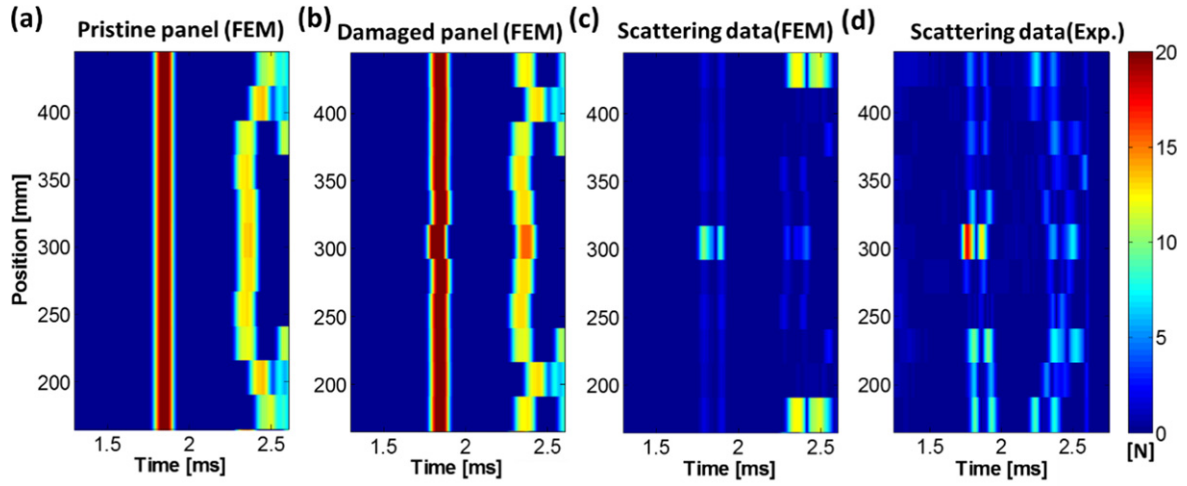

Figure 5. Image maps of the reflected solitary waves along the central inspection line. Numerical results obtained from (a) Pristine panel and (b) Damaged panel with artificial delamination. (c) Scattering of the two signals in (a) and (b). (d) Scattering signal obtained from experiments.

Given the parameters used in this study, we obtain the dimensionless contact time $\tau_c = 3.8$, corresponding to an actual contact time $T_c = 0.33$ ms. We find that this agrees well the contact time obtained from the FE simulation (0.34 ms) with 3% error.

We can calculate the traveling distance of flexural waves in the plate during the interaction time calculated above. The speed of these flexural waves can be expressed as follows:

$$c = k\sqrt{E_p/\rho_p}, \tag{4}$$

where the effective elastic modulus (E_p) is calculated to be 76.3 GPa from lamination theory [2] and k is a parameter that depends on the wave modes. The first antisymmetric Lamb wave mode (A0-mode) is the most dominant wave mode in the panel under the low frequency transverse excitations. The wave speed of the A0-mode depends on the wave frequency, and in the previous study, it has been shown that k is roughly 0.2 when the plate is excited by a solitary wave [21]. This results in the wave speed $c \approx 1300\,\mathrm{m\,s^{-1}}$, which agrees reasonably well with the wave speed estimated from the FE simulation ($c \approx 1200\,\mathrm{m\,s^{-1}}$). From these contact time and wave speed calculations, we can estimate a distance of flexural waves traveling during the interaction time between the granular crystal and the plate. The critical distance for which boundary effects do not affect the first wave reflection can be expresses as $L_c = cT_c/2$. Using the estimated contact time and wave speed, we obtain the critical distance as $L_c \simeq 210$ mm, which covers the fluctuating region of the TOF and amplitude ratio plots as seen in figures 4(a) and (b).

4.2. Inspection of delamination at the plate center

We investigate the delamination present in the center of the plate, located far enough from the boundary to avoid boundary effects (as discussed in the previous section). Figure 5 shows the numerical and experimental surface maps of the reflected solitary waves in the vicinity of the central delamination. As seen from the numerical results of the pristine plate (figure 5(a)), we confirm that the first reflected solitary wave is identical regardless of the measurement positions (see the red colored region around 1.8 ms in figure 5(a)). Note that this insensitivity cannot be found in the subsequent solitary waves (e.g., waves around 2.2 $\sim$ 2.5 ms), since these secondary reflections of the solitary waves are affected by the flexural waves reflected from the fixed boundaries of the plate. Once again, we focus only on the study of the primary reflected solitary waves, although investigation of the subsequent reflected solitary waves may provide additional, useful diagnostic information.

Figure 5(b) shows the FE results obtained from the damaged plate. We observe that the reflected solitary waves show a noticeable perturbation around $x = 300$ mm. This anomaly becomes more evident when we calculate the scattered signals, by subtracting the pristine panel's data from this damaged plate's signal (figure 5(c)). We observe pronounced scattering of reflected waves in positions corresponding to the location of the delamination defect. The experimental data presented in figure 5(d) corroborate the numerical result qualitatively.

It is interesting to note that the solitary wave reflected at the delamination point is stronger than the one obtained in the same position from the pristine panel. Similarly, we also find that its TOF is shorter than that from the pristine one. To understand this, we numerically compare the temporal force profiles at two interfaces: one between the 19th and the 20th spheres in the granular crystal sensor/actuator, and the other between the panel and the last sphere (20th sphere in the chain), as shown in figures 6(a) and (b) respectively. The pristine panel (solid curves) shows higher contact forces and the shorter contact times compared to those obtained in the damaged panel (dashed curves in figure 6(b)). This is because the delamination in the damaged panel reduces the local bending stiffness of the panel, which induces softer contact with larger deflections (see the inset of figure 6(b) for the displacement profiles at the contact interface). In the contact force profiles between the 19th and the 20th spheres, however, the damaged panel shows larger amplitude than that of

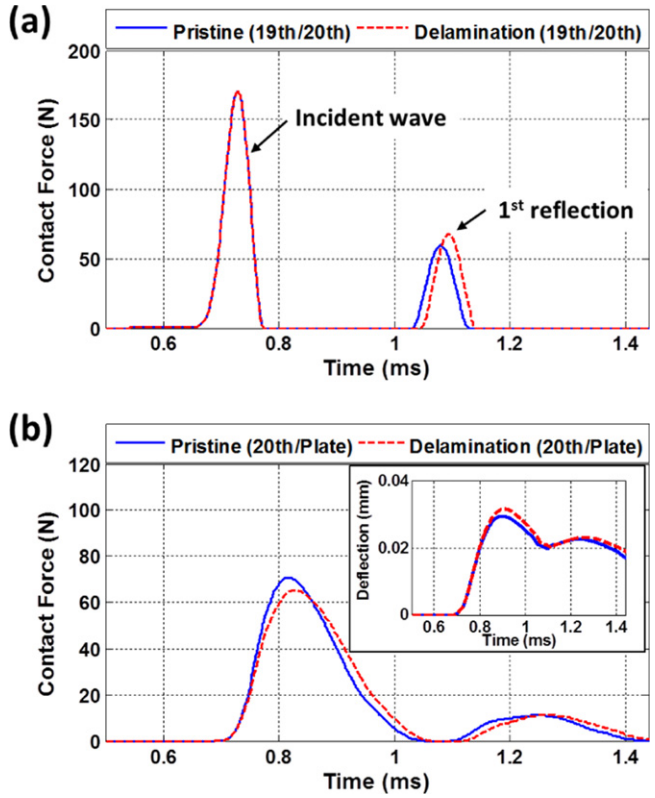

Figure 6. Contact forces (a) between 19th and 20th sphere and (b) between the last (20th) sphere and panel. Blue lines show the interaction with pristine panel and red lines show the interaction with the panel having artificial delamination. The inset in (b) shows displacement histories of the composite panel at the contact points.

the pristine panel in the first reflection (see the wave around 1.1 ms in figure 6(a)). This is because the damaged panel induces a larger momentum transmission to the granular crystal during the extended contact time, though its force magnitude is lower than that in pristine panel. By calculating the area under the first envelop of this force-time curve, we obtain that the transferred momentum is 0.0034 Nm for the damaged panel, which is approximately 10% larger than the pristine panels' momentum (0.0031 Nm). It should be noted that such larger magnitude of the reflected solitary wave leads to the reduction of TOF, because the speed of solitary wave depends on its amplitude as $V \propto F^{1/6}$, where V and F are the wave speed and amplitude, respectively [17, 22].

For the quantification of the solitary wave scattering, we define a damage index as below:

$$\mathrm{DI} = \left[\int_{T_{r1}}^{T_{r2}} \left[f_{\mathrm{refl}} \big|^{\mathrm{damage}} - f_{\mathrm{refl}} \big|^{\mathrm{pristine}} \right]^2 \mathrm{d}t \Big/ \int_{T_{i1}}^{T_{i2}} f_{\mathrm{in}}^2 \, \mathrm{d}t \right]^{1/2}, \tag{5}$$

where $f_{\mathrm{refl}}|^{\mathrm{damage}}$ and $f_{\mathrm{refl}}|^{\mathrm{pristine}}$ represent the force profiles of the solitary waves reflected from the damaged and pristine panels, and f_{in} denotes the incident solitary wave's profile which is identical for both damaged and pristine cases. For the calculation of this damage index, we accounted for the primary portion of the reflected waves (i.e., primary reflected wave). Thus, the time span of the integration in equation (5) needs to be from T_{r1} to T_{r2} for the reflected waves, which denote the beginning and ending of the first reflected wave. For the incident wave in the denominator of equation (5), the corresponding integration domain is from T_{i1} to T_{i2}, which encompasses the incident part of the propagating waves. In figure 7, we find that the damage indices from the FE simulation and the experiment show good agreement, denoting large peaks at the delamination position at $x = 305$ mm. However, the damage index from the experiment is smaller than that from the FE simulation. This is because the magnitude of the measured solitary wave is reduced by the damping in the system.

4.3. Inspection of delamination in the plate edge

In this section, we discuss the inspection of the delamination positioned at the panel boundary. Figures 8(a) and (b) show reflected solitary waves from the pristine panel and the damaged panel, respectively. As the inspection location is farther away from the boundary, the wave reflection becomes more delayed, as explained in section 4.1. Figures 8(c) and (d) show the scattering signals from the FE analysis and experiment, respectively. They qualitatively agree with each other, showing large signal scattering at the delamination locations (76.6 mm $\sim$ 102 mm). We compare the numerical and experimental damage index in figure 9, where we observe the increase of the damage index at the delamination positions. Notably, within the delamination region, the numerical damage index shows a decreasing trend as the inspection location becomes farther away from the fixed boundary. This could be due to the complex wave dynamics between the diagnostic solitary wave and the flexural waves that depart from and return to the inspection point within the interaction time between the granular crystal sensor/actuator and the delaminated composite plate. We find that this diagnostic approach based on solitary wave is highly site-specific, identifying the damage locations only when the delamination is located underneath the inspection positions. This could be a limiting factor for remote sensing purposes. However, if an inspection medium contains locally variant damage profiles, this site-specific nature of the solitary wave-based diagnostic scheme could be advantageous in identifying such damage.

5. Conclusions

In this study, we numerically and experimentally demonstrate a solitary wave-based diagnostic technique for the detection of delamination in the fiber-reinforced polymer composite panel. We generate diagnostic solitary wave using a combined sensor and actuator made of granular crystals. We inject solitary waves to specific spots of the composite plate and measure the reflected solitary waves using the same apparatus. We find that the reflection patterns of solitary waves are highly sensitive to the boundary conditions of the plate and the existence of hidden delamination. Particularly, we find

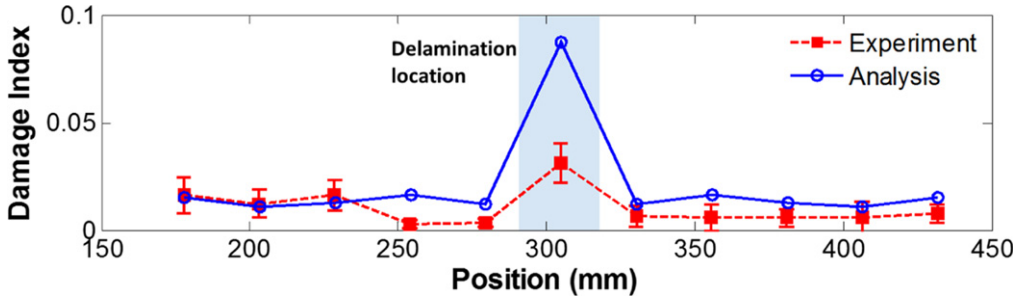

Figure 7. Comparison of the damage index for the central delamination inspections between the FE simulation (dashed curve with red squares) and the experiment result (solid curve with hollow circles).

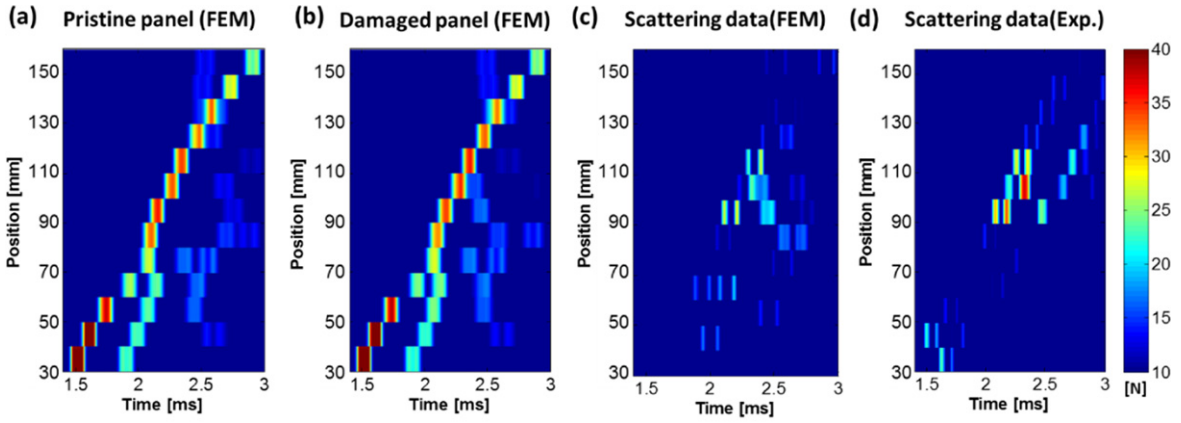

Figure 8. Image maps of the reflected solitary waves along the sideline inspection. Numerical results from (a) Pristine panel and (b) damaged panel with artificial delamination. (c) Scattering signals from the data in (a) and (b). (d) Scattering signals obtained from the experiments.

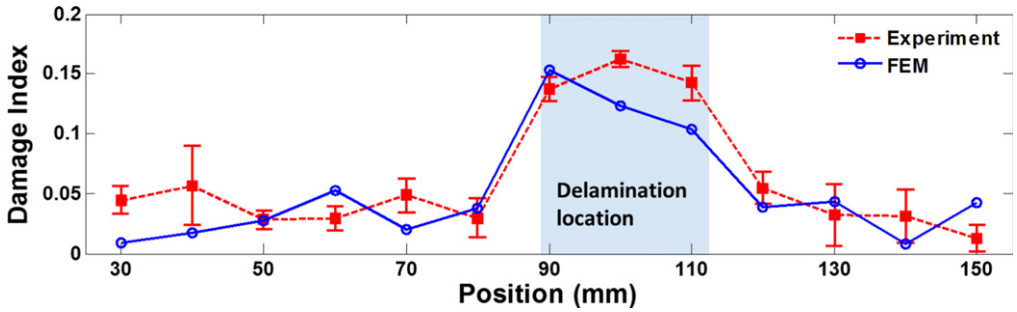

Figure 9. Comparison of the damage index from FE simulation with experiment along the side inspection line.

that the time-of-flight and the amplitude ratios of solitary waves reflected from the composite panel depend on the local stiffness of the composite panel. The change in local stiffness due to delamination can be identified by calculating the damage index based on the scattered profiles of reflected solitary waves. The solitary wave-based diagnostic scheme can provide unique advantages, such as site-specific and fast assessment of delamination. The granular crystal sensor also offers combined sensing and actuation capability and portability, which could be highly useful for hot spot monitoring of composite structures for aerospace and automotive applications. While this study focused on the analysis of the primary reflected solitary wave, further studies can be conducted for the investigation of subsequent reflected waves' profiles in relation to various types of composite damages and their characteristics (e.g., damage size).

Acknowledgments

We thank I Yoon for helping with the numerical analysis. J Yang and E Kim acknowledge the support from the US Office of Naval Research (N000141410388), National Science Foundation (CMMI- 1414748), and the Royalty Research Fund from the University of Washington. C Daraio acknowledges support from the US National Science Foundation (CMMI-1200319).

References

[1] Hahn H T and Tsai S W 1980 *Introduction to Composite Materials* (Lancaster, PA: Technomic Publishing Co, Inc.)

[2] Daniel I M and Ishai O 1994 *Engineering Mechanics of Composite Materials* (New York: Oxford University Press)
[3] Zou Y, Tong L and Steven G P 2000 Vibration-based model-dependent damage (delamination) identification and health monitoring for composite structures—a review *J. Sound Vib.* **230** 357–78
[4] Okafor A C, Chandrashekhara K and Jiang Y P 1996 Delamination prediction in composite beams with built-in piezoelectric devices using modal analysis and neural network *Smart Mater. Struct.* **5** 338–47
[5] Hoon S and Jun L S 2010 Lamb wave tuning curve calibration for surface-bonded piezoelectric transducers *Smart Mater. Struct.* **19** 015007
[6] Park G and Inman D J 2007 Structural health monitoring using piezoelectric impedance measurements *Phil. Trans. R. Soc.* A **365** 373–92
[7] Staszewski W J *et al* 1997 Wavelet signal processing for enhanced Lamb-wave defect detection in composite plates using optical fiber detection *Opt. Eng.* **36** 1877–88
[8] Kim S-W *et al* 2014 Damage evaluation and strain monitoring of composite plates using metal-coated FBG sensors under quasi-static indentation *Composites* B **66** 36–45
[9] Kim S-W *et al* 2011 Structural performance tests of down scaled composite wind turbine blade using embedded fiber bragg grating sensors *Int. J. Aeronaut. Space Sci.* **12** 346–53
[10] Qin Y and Bao N-K 1995 Thermographic nondestructuve testing (NDT) technique for delaminated defects in composite structures *Proc. SPIE* **2473** 219
[11] Adams R D and Cawley P 1988 A review of defect types and nondestructive testing techniques for composites and bonded joints *NDT Int.* **21** 208–22
[12] Hung Y Y 1999 Applications of digital shearography for testing of composite structures *Composites* B **30** 9
[13] Ostachowicz W, Radzieński M and Kudela P 2014 50th anniversary article: comparison studies of full wavefield signal processing for crack detection *Strain* **50** 275–91
[14] Khatri D, Rizzo P and Daraio C 2008 Highly nonlinear waves' sensor technology for highway inftrastructures *Proc. SPIE* **6934** 6934OU
[15] Ni X, Rizzo P and Daraio C 2011 Actuators for the generation of highly nonlinear solitary waves *Rev. Sci. Instrum.* **82** 034902–6
[16] Yang J *et al* 2012 Site-specific quantification of bone quality using highly nonlinear solitary waves *J. Biomech. Eng* **134** 101001
[17] Nesterenko V F 2001 *Dynamics of Heterogeneous Materials* (New York: Springer)
[18] Sen S *et al* 2008 Solitary waves in the granular chain *Phys. Rep.* **462** 21–66
[19] Spadoni A and Daraio C 2010 Generation and control of sound bullets with a nonlinear acoustic lens *Proc. Natl Acad. Sci. USA* **107** 7230–4
[20] Job S *et al* 2005 How Hertzian solitary waves interact with boundaries in a 1D granular medium *Phys. Rev. Lett.* **94** 178002
[21] Yang J *et al* 2012 Interaction of highly nonlinear solitary waves with thin plates *Int. J. Solids Struct.* **49** 1463–71
[22] Yang J *et al* 2011 Interaction of highly nonlinear solitary waves with linear elastic media *Phys. Rev.*E **83** 046606
[23] Aggen C *et al* 1990 *Properties and Selection: Irons, Steels, and High-Performance Alloys* (*Metals Handbook*) vol 1 ed K M Zwilsky *et al* (10th ed.; New York: ASM International Handbook Committee)
[24] Daraio C *et al* 2005 Strongly nonlinear waves in a chain of Teflon beads *Phys. Rev.* E **72** 016603
[25] Kim E-H *et al* 2013 Composite damage model based on continuum damage mechanics and low velocity impact analysis of composite plates *Compos. Struct.* **95** 123–34
[26] Khatri D, Ngo D and Daraio C 2011 Highly nonlinear solitary waves in chains of cylindrical particles *Granular Matter* **14** 63–9
[27] Johnson K L 1985 *Contact Mechanics* (Cambridge: Cambridge University Press)
[28] Sondergaard R, Chaney K and Brennen C E 1990 Measurements of solid spheres bouncing off flat plates *J. Appl. Mech.* **57** 694–9
[29] Zener C 1941 The intrinsic inelasticity of large plates *Phys. Rev.* **59** 669
[30] Daraio C, Nesterenko V and Jin S 2004 Strongly nonlinear waves in 3D phononic crystals *AIP Conf. Proc.* **706** 197–200
[31] Chatterjee A 1999 Asymptotic solution for solitary waves in a chain of elastic spheres *Phys. Rev.* E **59** 5912–9
[32] Job S *et al* 2007 Solitary wave trains in granular chains: experiments, theory and simulations *Granular Matter* **10** 13–20